




Inverse cascading for initial magnetohydrodynamic turbulence spectra between Saffman and Batchelor

Axel Brandenburg ^{1,2,3,4,†}, Ramkishor Sharma ^{1,2} and Tanmay Vachaspati ^{5,6}

¹Nordita, KTH Royal Institute of Technology and Stockholm University, Hannes Alfvéns väg 12, SE-10691 Stockholm, Sweden

²The Oskar Klein Centre, Department of Astronomy, Stockholm University, AlbaNova, SE-10691 Stockholm, Sweden

³McWilliams Center for Cosmology & Department of Physics, Carnegie Mellon University, Pittsburgh, PA 15213, USA

⁴School of Natural Sciences and Medicine, Ilia State University, 3-5 Cholokashvili Avenue, 0194 Tbilisi, Georgia

⁵Physics Department, Arizona State University, Tempe, AZ 85287, USA

⁶Département de Physique Théorique and Centre for Astroparticle Physics, Université de Genève, 24 quai Ernest-Ansermet, CH-1211 Genève 4, Switzerland

(Received 10 July 2023; revised 6 November 2023; accepted 8 November 2023)

In decaying magnetohydrodynamic (MHD) turbulence with a strong magnetic field, the spectral magnetic energy density is known to increase with time at small wavenumbers k , provided the spectrum at low k is sufficiently steep. This process is called inverse cascading and occurs for an initial Batchelor spectrum, where the magnetic energy per linear wavenumber interval increases like k^4 . For an initial Saffman spectrum that is proportional to k^2 , however, inverse cascading has not been found in the past. We study here the case of an intermediate k^3 spectrum, which may be relevant for magnetogenesis in the early Universe during the electroweak epoch. This case is not well understood in view of the standard Taylor expansion of the magnetic energy spectrum for small k . Using high resolution MHD simulations, we show that, also in this case, there is inverse cascading with a strength just as expected from the conservation of the Hosking integral, which governs the decay of an initial Batchelor spectrum. Even for shallower k^α spectra with spectral index $\alpha > 3/2$, our simulations suggest a spectral increase at small k with time t proportional to $t^{4\alpha/9-2/3}$. The critical spectral index of $\alpha = 3/2$ is related to the slope of the spectral envelope in the Hosking phenomenology. Our simulations with 2048^3 mesh points now suggest inverse cascading even for an initial Saffman spectrum.

Key words: astrophysical plasmas

† Email address for correspondence: brandenb@nordita.org

1. Introduction

Standard hydrodynamic turbulence exhibits forward cascading whereby kinetic energy cascades from large scales (small wavenumbers) to smaller scales (larger wavenumbers) (Kolmogorov 1941). This also happens in decaying turbulence, except that the rate of energy transfer to smaller scales is here decreasing with time (Batchelor 1953; Saffman 1967). In magnetohydrodynamic (MHD) turbulence, the situation is in many ways rather different. This is primarily owing to magnetic helicity (Hosking & Schekochihin 2021), which is a conserved quantity in the absence of magnetic diffusivity (Woltjer 1958). Magnetic helicity is an important property of MHD turbulence that is not shared with hydrodynamic turbulence, even though there is kinetic helicity that is also an invariant if viscosity is strictly vanishing (Moffatt 1969). However, this is no longer true when the viscosity is finite (Matthaeus & Goldstein 1982). This is because kinetic helicity dissipation occurs faster than kinetic energy dissipation, whereas magnetic helicity dissipation occurs more slowly than magnetic energy dissipation for finite magnetic diffusivity (Berger 1984).

The importance of magnetic helicity conservation has been recognized long ago by Frisch *et al.* (1975) and Pouquet, Frisch & Leorat (1976) in cases when it is finite on average. In that case, it leads to the phenomenon of an inverse cascade. In forced turbulence, this means that part of the injected energy gets transferred to progressively larger scales (Brandenburg 2001). This process is at the heart of large-scale dynamos, which can be described by what is known as the alpha effect (Steenbeck, Krause & Rädler 1966), and is relevant for explaining the large-scale magnetic fields in stars and galaxies (Parker 1979). In decaying MHD turbulence, on the other hand, inverse cascading leads to a temporal increase of the magnetic energy at the smallest wavenumbers. A similar phenomenon has never been seen in hydrodynamic turbulence, where the spectrum at small k remains unchanged.

Even when the magnetic helicity vanishes on average, there can still be an inverse cascade. In that case, it is no longer the mean magnetic helicity density whose conservation is important, but the magnetic helicity correlation integral, also known as the Hosking integral (Hosking & Schekochihin 2021; Schekochihin 2022; Zhou, Sharma & Brandenburg 2022). In non-helical turbulence, the possibility of inverse cascading with an increase of spectral magnetic energy at small wavenumbers was originally only seen for steep initial magnetic energy spectra, $E_M(k) \propto k^4$, where k is the wavenumber. Here, $E_M(k)$ is defined as the spectral magnetic energy per linear wavenumber interval and is normalized such that $\int E_M(k, t) dk = \langle \mathbf{B}^2 \rangle / 2 \equiv \mathcal{E}_M(t)$ is the mean magnetic energy density. Those k^4 spectra were motivated by causality arguments, requiring that magnetic field correlation functions strictly vanish outside the light cone (Durrer & Caprini 2003). Such a field can be realized by a random vector potential that is δ -correlated in space, i.e. the values of any two neighbouring mesh points are completely uncorrelated. The magnetic vector potential \mathbf{A} therefore has a k^2 spectrum, which implies that the magnetic field $\mathbf{B} = \nabla \times \mathbf{A}$ has a k^4 spectrum.

For the case of a shallower $E_M(k) \propto k^2$ spectrum, no inverse cascade has been found (Brandenburg *et al.* 2017; Reppin & Banerjee 2017). This was explained by the conservation of the magnetic Saffman integral (Brandenburg & Larsson 2023), which constitutes the coefficient in the leading quadratic term of the Taylor expansion of the magnetic energy spectrum for small k .

The intermediate case of a k^3 spectrum may be realized during the electroweak epoch in cosmology due to a distribution of magnetic charges as shown in Vachaspati (2021) and Patel & Vachaspati (2022). The evolution of the magnetic field in this case is less clear.

Reppin & Banerjee (2017) reported weak inverse cascading, but it is not obvious whether this agrees with what should be expected based on the conservation of the Hosking integral, or whether it is some intermediate case in which the possible conservation of both the magnetic Saffman integral and also the Hosking integral can play a role. Investigating this in more detail is the purpose of the present work.

2. Preliminary considerations

2.1. Relevant integral quantities in MHD

Three important integrals have been discussed in the context of decaying MHD turbulence. The first two are the magnetic Saffman and magnetic Loitsyansky integrals (Hosking & Schekochihin 2021)

$$I_{SM} = \int \langle \mathbf{B}(\mathbf{x}) \cdot \mathbf{B}(\mathbf{x} + \mathbf{r}) \rangle d^3r, \tag{2.1}$$

$$I_{LM} = - \int \langle \mathbf{B}(\mathbf{x}) \cdot \mathbf{B}(\mathbf{x} + \mathbf{r}) \rangle r^2 d^3r, \tag{2.2}$$

respectively. Here, angle brackets denote ensemble averages, which we approximate by volume averages. The integrals (2.1) and (2.2) are analogous to those in hydrodynamics, but with \mathbf{B} being replaced by the velocity \mathbf{u} . The third relevant quantity is the Hosking integral (Hosking & Schekochihin 2021; Schekochihin 2022)

$$I_H = \int \langle h(\mathbf{x})h(\mathbf{x} + \mathbf{r}) \rangle d^3r, \tag{2.3}$$

where $h = \mathbf{A} \cdot \mathbf{B}$ is the magnetic helicity density. By defining the longitudinal correlation function $M_L(r)$ through

$$\langle \mathbf{B}(\mathbf{x}) \cdot \mathbf{B}(\mathbf{x} + \mathbf{r}) \rangle = \frac{1}{r^2} \frac{d}{dr} (r^3 M_L), \tag{2.4}$$

the integrals I_{SM} and I_{LM} emerge as the coefficients of the Taylor expansion of the magnetic energy (Subramanian 2019). A similar expansion also applies to the magnetic helicity variance spectra (Hosking & Schekochihin 2021).

For power spectra that decay sufficiently rapidly, a Taylor expansion of $(kr)^{-1} \sin kr$ gives

$$\text{Sp}(\mathbf{B})|_{k \rightarrow 0} = \frac{2k^2}{\pi} \int \frac{d}{dr} (r^3 M_L) \left(1 - \frac{k^2 r^2}{6} + \dots \right) dr \equiv \frac{I_{SM}}{2\pi^2} k^2 + \frac{I_{LM}}{12\pi^2} k^4 + \dots, \tag{2.5}$$

$$\text{Sp}(h)|_{k \rightarrow 0} = \frac{I_H}{2\pi^2} k^2 + \dots. \tag{2.6}$$

Here, $\text{Sp}(h) = (k^2/8\pi^3 L^3) \oint_{4\pi} |\tilde{h}|^2 d\Omega_k$ is the shell-integrated spectrum in volume L^3 , the tilde marks a quantity in Fourier space and Ω_k is the solid angle in Fourier space, so that $\int \text{Sp}(h) dk = \langle h^2 \rangle$, and likewise for $\int \text{Sp}(\mathbf{B}) dk = \langle \mathbf{B}^2 \rangle$. The definition of shell integration implies that Parseval's theorem in the form $\langle h^2 \rangle L^3 = \int |\tilde{h}|^2 d^3k / (2\pi)^3$ is obeyed. The magnetic energy spectrum is defined as $E_M(k, t) = \text{Sp}(\mathbf{B})/2\mu_0$, where μ_0 is the magnetic permeability, but in the following, we measure \mathbf{B} in units where μ_0 is set to unity.

According to (2.5), $\text{Sp}(\mathbf{B})$ seems to be constrained to having only even powers of k in the limit $k \rightarrow 0$. Furthermore, $\text{Sp}(\mathbf{B}) \propto k^2$ when I_{SM} is finite and dominant, and likewise,

$\text{Sp}(\mathbf{B}) \propto k^4$ when I_{LM} is finite and dominant. The expansion in powers of k in (2.5) holds, however, only when the coefficients in the expansion are finite. This is the case if, for example, M_L is an exponentially decaying function of r . If, on the other hand, M_L decays only as a power law, the expansion does not hold since higher-order coefficients will be divergent. In such cases the leading-order behaviour in k may consist of odd (or even arbitrary) powers of k . A simple counterexample to the expansion in (2.5) is provided by considering the case $r^3 M_L \propto r$ for large r in (2.4). The specific case of $\text{Sp}(\mathbf{B}) \propto k^3$ occurs for magnetic fields produced during electroweak symmetry breaking as discussed in Vachaspati (2021) and Patel & Vachaspati (2022).

2.2. Competition between I_{SM} and I_H

Using the Taylor expansion of the magnetic energy spectrum in (2.5), we see that, for initial Saffman scaling ($E_M \propto k^\alpha$ with $\alpha = 2$), the magnetic Saffman integral I_{SM} must be non-vanishing. For initial Batchelor scaling ($\alpha = 4$), on the other hand, I_{SM} vanishes initially and cannot play a role. In that case, the conservation of I_H becomes important and leads to inverse cascading, which then also implies the non-conservation of I_{SM} (Hosking & Schekochihin 2021).

Our question here is what happens in the intermediate case when $\alpha = 3$, a case already discussed in the supplemental material of Hosking & Schekochihin (2023). In that situation, $\text{Sp}(\mathbf{B})$ and $\text{Sp}(h)$ cannot be Taylor expanded and it is unclear whether there is then inverse cascading, because it would require violation of the conservation of I_{SM} , or whether I_{SM} is conserved, as for $\alpha = 2$, and there is no inverse cascade.

2.3. Growth of spectral energy at small wavenumbers

We now want to quantify the growth of spectral energy at small wavenumbers. As in Brandenburg & Kahnishvili (2017), we use self-similarity, i.e. the assumption that the magnetic energy spectra at different times can be collapsed on top of each other by suitable rescaling. Thus, we write

$$E_M(k, t) = \xi_M^{-\beta} \phi(\xi_M k), \quad (2.7)$$

where $\xi_M(t) = \int k^{-1} E_M(k) dk / \mathcal{E}_M$ is the integral scale and β depends on the relevant conservation law: $\beta = 2$ for Saffman scaling and $\beta = 3/2$ for Hosking scaling. This follows from the dimensions of the conserved quantity; see Brandenburg & Larsson (2023) for details. Next, we assume a certain initial subinertial range scaling, $E_M(k, 0) = a_{\alpha 0} k^\alpha$, where $a_{\alpha 0}$ is a coefficient determining the initial field strength. Thus, for $k \xi_M \ll 1$, we can write $\phi = a_{\alpha 0} (\xi_M k)^\alpha$, so

$$E_M(k, t) = a_\alpha \xi_M^{\alpha-\beta} k^\alpha \quad (k \xi_M \ll 1). \quad (2.8)$$

Assuming power-law scaling, $\xi_M(t) \propto t^q$, we get

$$\lim_{k \rightarrow 0} E_M(k, t) \propto t^{(\alpha-\beta)q}. \quad (2.9)$$

From this, it follows that inverse cascading is possible for $\alpha > \beta$, so $\alpha = 2$ and $\beta = 3/2$ could, in principle, still give rise to inverse cascade.

Following Brandenburg & Kahnishvili (2017), who assumed a self-similar decay, we have $q = 2/(\beta + 3)$, so $q = 2/5$ for $\beta = 2$ and $q = 4/9$ for $\beta = 3/2$; see table 1 for a comparison of different theoretical possibilities for the various exponents. Thus, unless I_{SM} were conserved and there were therefore no inverse cascades, we must expect $\lim_{k \rightarrow 0} E_M(k, t) \propto t^{2/3}$ for cubic scaling ($E_M \propto k^3$, i.e. between Saffman and Batchelor

α	β	q	$(\alpha - \beta)q$	comment, property
1.7	3/2	4/9	4/45 \approx 0.09	non-integer scaling, assuming Hosking integral conserved
2	2	2/5	0	Saffman scaling, assuming Saffman integral conserved
2	3/2	4/9	2/9 \approx 0.22	Saffman scaling, assuming Hosking integral conserved
2.5	3/2	4/9	4/9 \approx 0.44	non-integer scaling, assuming Hosking integral conserved
3	3/2	4/9	2/3 \approx 0.67	cubic scaling, assuming Hosking integral conserved
4	3/2	4/9	10/9 \approx 1.11	Batchelor scaling, assuming Hosking integral conserved
6	3/2	4/9	(2)	very blue spectrum

TABLE 1. Summary of $(\alpha - \beta)q$ for Saffman ($\alpha = 2$), Batchelor ($\alpha = 4$) and intermediate ($1.7 \leq \alpha \leq 3$) spectra under the assumption that either the Saffman integral is conserved ($\beta = 2$) or the Hosking integral ($\beta = 3/2$). Two non-integer values of α are also considered. For $\alpha = 6$, the subinertial range quickly becomes shallower with time, so the value $(\alpha - \beta)q = 2$ does not apply and is put in parentheses.

scalings) when the Hosking integral is conserved ($\beta = 3/2$ and $q = 4/9$). Let us also note that the case $\alpha > 4$ reduces to that of $\alpha = 4$ after a short time; see [Appendix A](#). In the following, however, we present numerical simulations demonstrating that, for $3/2 < \alpha \leq 4$, there is indeed inverse cascading with the expected rise of spectral magnetic energy at small values of k . We focus on the $\alpha = 3$, but we also consider $\alpha \neq 3$ to show that an inverse cascade always occurs for $\alpha > 3/2$ and that the Hosking integral is conserved.

3. Simulations

We perform simulations in a domain of size $(2\pi)^3$, so the lowest non-vanishing wavenumber is $k \equiv k_1$. For most runs, we use $k_1 = 1$, but we use $k_1 = 0.02$ for what we call runs A and D. For the run with $\alpha = 3$ (run B), as well as for all other runs, we assume that the initial magnetic energy spectrum peaks at $k_0 = 60k_1$, and therefore we consider spectral values for $k = k_1$ to approximate the limit $k \rightarrow 0$. We use $N^3 = 2048^3$ mesh points in all those simulations, so the largest wavenumber is 1024. This is similar to a run of Zhou *et al.* (2022) with $\alpha = 4$, which is here called run C. We also compare with some other runs that we discuss later. All simulations are performed with the PENCIL CODE (Pencil Code Collaboration *et al.* 2021), which solves the compressible, isothermal equations using sixth-order finite differences and a third-order time stepping scheme.

In the numerical simulations, the sound speed c_s is always chosen to be unity, i.e. $c_s = 1$. The initial position of the spectral peak is at $k = k_0$ and its numerical value is chosen to be 60 and the lowest wavenumber in the domain is unity, or, when using the data of Brandenburg & Larsson (2023), $k_0 = 1$ and $k_1 = 0.02$, so that $k_0/k_1 = 50$. The magnetic diffusivity is $\eta k_1/c_s = 2 \times 10^{-6}$ in runs B and C, so $\eta k_0/c_s = 1.2 \times 10^{-4}$. In some runs with $\alpha = 2$, we also present results for larger values of η . The magnetic Prandtl number, i.e. the ratio of kinematic viscosity ν to magnetic diffusivity, $\text{Pr}_M = \nu/\eta$, is unity for most of our runs. For runs A and D, we have $\eta k_0/c_s = 5 \times 10^{-5}$ and $\nu k_0/c_s = 2 \times 10^{-4}$, so $\text{Pr}_M = 4$.

Neither hyperviscosity nor magnetic hyperdiffusivity are used in any of our runs. Hyperviscosity and magnetic hyperdiffusivity are sometimes used to enhance the length of the inertial range. This would give rise to different scalings, as explained in the works of Hosking & Schekochihin (2021) and Zhou *et al.* (2022). This led to the idea that a finite reconnection time could significantly prolong the decay (Zhou *et al.* 2019; Zhou, Loureiro

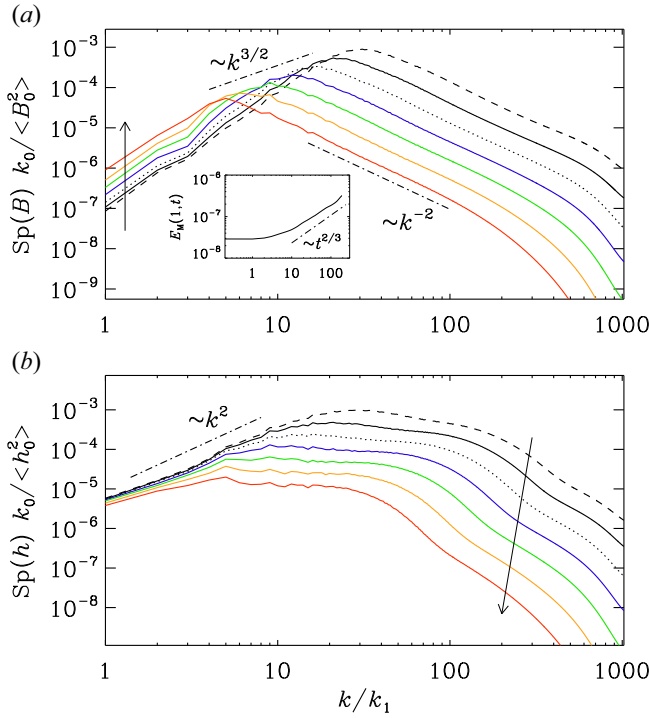


FIGURE 1. (a) Values of $E_M(k, t)$ and (b) $Sp(h)$ vs k for run B with $\alpha = 3$ at $t = 2, 5, 10, 25, 50, 100$ and 200 . The first three times are shown as black dashed, solid and dotted lines. The next four times are shown as solid blue, green, orange and red lines. The upward arrow in (a) indicates the direction of time. The inset in (a) shows that $E_M(k_1, t) \propto t^{2/3}$.

& Uzdensky 2020; Bhat, Zhou & Loureiro 2021). However, this aspect will not be pursued in the present paper.

The initial magnetic field strength is characterized by the Alfvén speed $v_A \equiv B_{rms}/\sqrt{\rho}$, where ρ is the gas density. For most of our runs, we choose rather strong magnetic fields with an initial value $v_{A0}/c_s \approx 0.87$.

3.1. Inverse cascading

The results for the magnetic energy and helicity variance spectra are shown in figure 1, which shows inverse cascading with $E_M(k_1, t) \propto t^{2/3}$ and $Sp(h) = \text{const.}$ for $k \rightarrow 0$. The temporal increase at low k is compatible with table 1 for $\alpha = 3, \beta = 3/2, q = 4/9$, and thus $(\alpha - \beta)q = 2/3$. For general values $3/2 \leq \alpha \leq 4$, the spectral increase at small k is proportional to $t^{4\alpha/9 - 2/3}$.

In the supplemental material of Hosking & Schekochihin (2023), it was proposed that the evolution for $\alpha \leq 3$ deviates from self-similarity at intermediate times, and that the spectrum might show a ‘pile up’ to the left of the peak where it would locally be approaching k^4 scaling. In fact, this was already proposed by Vachaspati (2021, see his figure 16). While we cannot exclude the possibility of a short k^4 range, figure 1(a) suggests that such a tendency could at best be identified at intermediate times. However, according to the phenomenology of Hosking & Schekochihin (2023), this range should become wider at later times. This is certainly not the case in the simulations, but there is the worry that, at

late times, our results become affected by finite-size effects; see the blue and green curves for $t = 25$ and 50 , respectively.

At early times, our simulations are poorly resolved and one might wonder whether they are then still reliable. Poor resolution can be seen by the lack of a proper dissipation range in [figure 1\(a\)](#) for $t = 2$. At later times, however, the simulations are certainly well resolved and inverse cascading is still found to persist. Thus, we argue that the initial phase does not adversely affect our results. Indeed, sufficiently small viscosity and magnetic diffusivity are crucial for being able to verify the expected Hosking scaling.

Next, we compare in [figure 2](#) compensated spectra, which allow us to determine $a_\alpha = \text{Sp}(\mathbf{B})/2k^\alpha$ and $I_H \rightarrow 2\pi^2 \text{Sp}(h)/k^2$ for small k , where the k -dependence of those compensated spectra is approximately flat. The fact that the magnetic Saffman integral is not conserved is evidenced by the increase in the height $a_\alpha(t)$ of the compensated magnetic spectra; see [figure 2\(a,b\)](#). Only for $\alpha = 2$ does the height stay nearly constant, as was already verified by Brandenburg & Larsson (2023). In that case, we have $I_{\text{SM}} = 4\pi^2 a_2$. However, we return to this aspect in § 3.6, where our higher resolution simulations now suggest that, even in that case, the decay is governed by the conservation of the Hosking integral rather than the magnetic Saffman integral.

In [figure 2\(d\)](#), we see that $\text{Sp}(h)$ shows a distinctly downward trend with k for the smallest k values. This suggests that the conservation property of I_H begins to deteriorate, especially at late times. To clarify this further, even more scale separation would be useful, i.e. a run with a larger value of k_0 . Such runs at a resolution of 2048^3 mesh points are, however, rather expensive, but it is interesting to note that, even for the case of an initial k^4 spectrum, the compensated spectra show a similar downward trend with k when the numerical resolution is only 1024^3 ; see [figure 3\(d\)](#) of Brandenburg & Larsson (2023), which corresponds to our run D. It should also be noted that, in [figure 2\(d\)](#), the last time is $t = 190/c_s k_1$, while, in [figure 2\(c\)](#), the last time is only 60. The two times correspond to $t \eta k_0^2 \approx 1.4$ and 0.4 , respectively.

3.2. Universal scaling constants

Given that I_H is reasonably well conserved and enters the evolution of magnetic energy and correlation length, as well as the spectral envelope of the peak, through dimensional arguments, it is useful to determine the non-dimensional coefficients in these relations. This was done recently for the cases $\alpha = 2$ and $\alpha = 4$; see Brandenburg & Larsson (2023), who computed the coefficients $C_H^{(\xi)}$, $C_H^{(\mathcal{E})}$ and $C_H^{(E)}$, defined through the relations

$$\xi_M(t) = C_i^{(\xi)} I_i^\sigma t^q, \quad \mathcal{E}_M(t) = C_i^{(\mathcal{E})} I_i^{2\sigma} t^{-p}, \quad E_M(k) = C_i^{(E)} I_i^{(3+\beta)/\sigma} (k/k_0)^\beta, \quad (3.1a-c)$$

where the index i in the integrals I_i and the coefficients $C_i^{(\xi)}$, $C_i^{(\mathcal{E})}$ and $C_i^{(E)}$ stands for SM or H for magnetic Saffman and Hosking scalings, respectively, and σ is the exponent with which length enters in I_i : $\sigma = 5$ for the magnetic Saffman integral ($i = \text{SM}$) and $\sigma = 9$ for the Hosking integral ($i = \text{H}$). In the following, we focus on the case $i = \text{H}$, but refer to Brandenburg & Larsson (2023) for comparisons with $i = \text{SM}$. We recall that k_0 is the initial position of the spectral peak. Note that the last expression of (3.1a-c) describes an envelope under which $E(k, t)$ evolves; see [figure 1\(a\)](#) for an example.

In principle, the non-dimensional coefficients $C_H^{(\xi)}$, $C_H^{(\mathcal{E})}$ and $C_H^{(E)}$ could depend on other quantities characterizing the system, for example the magnetic Reynolds number, but they may also be universal, just as for the Kolmogorov constant in the kinetic energy spectrum. To begin assessing the degree of universality of these non-dimensional coefficients, we now consider the empirical laws $\xi_M(t)$, $\mathcal{E}_M(t)$ and $E_M(k, t)$ for the new case of $\alpha = 3$.

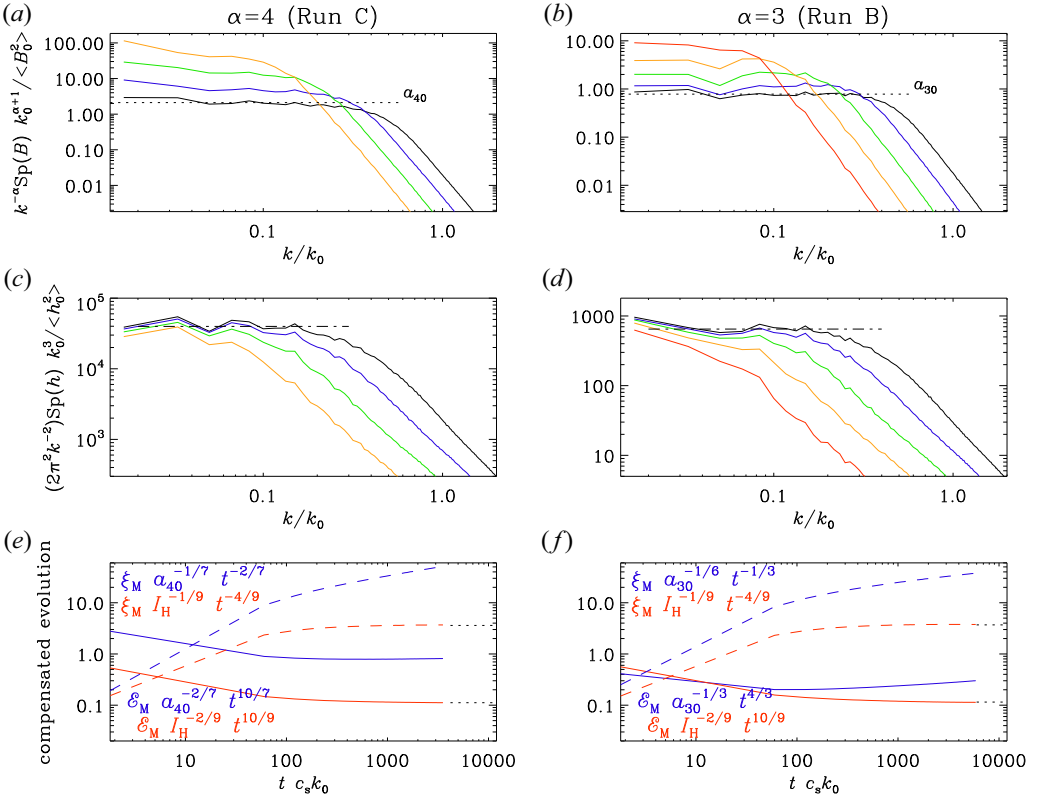


FIGURE 2. Compensated spectra showing that $\lim_{k \rightarrow 0} \text{Sp}(\mathbf{B})/k^\alpha$ is not constant, and that instead the Hosking integral is conserved. Panels (a,c,e) and (b,d,f) show a comparison between $\alpha = 4$ (Batchelor spectrum, a,c,e) and $\alpha = 3$ (b,d,f). The times are $t = 2$ (black), 6 (blue), 20 (green), 60 (orange) and 190 (red). For $\alpha = 4$ (a,c,e), $t = 190$ is not available. In panels (e,f), we see that the red lines asymptote to constants, compatible with earlier work (Brandenburg & Larsson 2023). In (e,f), the dashed curves denote the compensated time dependences of $\xi_M(t)$ and the solid ones refer to the compensated dependences of $\mathcal{E}_M(t)$. Thus, we plot $\xi_M I_H^{-1/9} t^{-4/9}$ and $\mathcal{E}_M I_H^{-2/9} t^{10/9}$, which are non-dimensional and should approach constants. The dotted lines mark the approximate positions of the asymptotic values of the non-dimensional constants in the Hosking scalings.

As in earlier work, the non-dimensional constants in the scaling laws for $\alpha = 3$ agree with those found earlier for $\alpha = 4$ (Brandenburg & Larsson 2023). Specifically, we have

$$\xi_M(t) \approx 0.12 I_H^{1/9} t^{4/9}, \quad \mathcal{E}_M(t) \approx 3.7 I_H^{2/9} t^{-10/9}, \quad E_M(k, t) \lesssim 0.025 I_H^{1/2} (k/k_0)^{3/2}. \tag{3.2a-c}$$

The quality of these asymptotic laws can be seen from the red lines in figure 2(e,f). The blue lines show the case if the Saffman integral were conserved. As explained above, those are based on the values of $a_{\alpha 0}$ indicated in figure 2(a,b). A comparison of the coefficients with those found by Brandenburg & Larsson (2023) is given in table 2. Note that, in figure 2(e,f), the solid and dashed blue lines show an asymptotic upward trend, reflecting again that the magnetic Saffman integral is not conserved.

Run	α	$C_H^{(\xi)}$	$C_H^{(\mathcal{E})}$	$C_H^{(E)}$	$\eta k_0/c_s$	$\mathcal{E}_M^2 \xi_M^5 k_0^5 / (\bar{\rho} c_s^2)^2$	I_H/I_H^{ref}	resol.
O	1.7	0.14	3.8	0.038	7×10^{-3}	1.1×10^{-2}	3.5	2048 ³
Q	2	0.13	3.7	0.038	7×10^{-3}	1.9×10^{-3}	6.3	2048 ³
A	2	0.15	3.8	(0.04)	5×10^{-5}	1.2×10^{-5}	6.5	1024 ³
A1	2	0.18	2.1	(0.04)	2×10^{-4}	1.7×10^{-5}	4.3	512 ³
A2	2	0.24	0.8	(0.04)	1×10^{-3}	1.7×10^{-5}	3.0	512 ³
P	2.5	0.12	3.9	0.038	7×10^{-3}	2.8×10^{-3}	9.6	2048 ³
B	3	0.12	3.7	0.025	7×10^{-3}	1.7×10^{-3}	12.2	2048 ³
C	4	0.11	3.6	0.037	7×10^{-3}	9.4×10^{-4}	8.3	2048 ³
D	4	0.13	3.5	0.037	5×10^{-5}	4.5×10^{-6}	17.5	1024 ³

TABLE 2. Summary comparison of the coefficients in the relations for $\xi_M(t)$, $\mathcal{E}_M(t)$ and $E_M(k, t)$ for different values of α . The numbers in parentheses indicate that the slope β is incompatible with the value of α .

3.3. The normalized Hosking integral

The runs of Brandenburg & Larsson (2023) had different mean magnetic energy densities and also the minimum wavenumber k_1 was not unity, but $k_1 = 0.02$, unlike the present cases, where $k_1 = 1$. Instead, the peak of the initial spectrum, k_0 , was then chosen to be unity. To compare such different runs, it is necessary to normalize I_{SM} and I_H appropriately. On dimensional grounds, I_{SM} is proportional to $\mathcal{E}_M \xi_M^3$ and I_H is proportional to $\mathcal{E}_M^2 \xi_M^5$. By approximating the spectrum as a broken power law, as in Zhou *et al.* (2022),

$$E_M(k) = \begin{cases} E_{\text{peak}} (k/k_{\text{peak}})^\alpha, & k \leq k_{\text{peak}}, \\ E_{\text{peak}} (k/k_{\text{peak}})^{-s}, & k > k_{\text{peak}}, \end{cases} \quad (3.3)$$

where $s = 5/3$ and $s = 2$ were used to represent the inertial range slopes at early and late times, respectively, we find

$$k_{\text{peak}} \xi_M = \frac{\alpha^{-1} + s^{-1}}{(\alpha + 1)^{-1} + (s - 1)^{-1}}, \quad E_{\text{peak}} = \frac{\mathcal{E}_M \xi_M}{\alpha^{-1} + s^{-1}}. \quad (3.4a,b)$$

For $\alpha = 2$, we find the following reference values for the Saffman integral:

$$I_{SM}^{\text{ref}} = 2\pi^2 \times \begin{cases} 250/99 & (\text{for } s = 5/3), \\ 16/9 & (\text{for } s = 2). \end{cases} \quad (3.5)$$

For other values of α , the value of I_{SM}^{ref} is not meaningful and only I_H^{ref} is computed for other values of α by using equations (2.14) and (4.5) in Zhou *et al.* (2022). It is given by

$$I_H^{\text{ref}} = 8\pi^2 \mathcal{E}_M^2 \xi_M^5 \left(\frac{(\alpha + 1)^{-1} + (s - 1)^{-1}}{(\alpha^{-1} + s^{-1})^{5/3}} \right)^3 \left(\frac{1}{2\alpha - 3} + \frac{1}{2s + 3} \right). \quad (3.6)$$

In calculating the above expression, we assumed the magnetic field distribution to be Gaussian and its spectrum to be of the form as given in (3.3). These reference values are summarized in table 3.

In table 2, we list the ratio I_H/I_H^{ref} , where $I_H^{\text{ref}} \propto \mathcal{E}_M^2 \xi_M^5$ is given in table 3. We have used here the actual values of α and $s = 2$ in all cases, which describes the late time inertial

α	s	$I_{SM}^{ref}/(\mathcal{E}_M \xi_M^3)$	$I_H^{ref}/(\mathcal{E}_M^2 \xi_M^5)$
1.7	5/3	—	$2\pi^2 4\,437\,053\,125/151\,086\,708 \approx 579.7$
1.7	2	—	$2\pi^2 90\,870\,848/5\,097\,897 \approx 351.9$
2	5/3	$2\pi^2 250/99 \approx 49.8$	$2\pi^2 100\,000/5643 \approx 349.8$
2	2	$2\pi^2 16/9 \approx 35.1$	$2\pi^2 2048/189 \approx 213.9$
2.5	5/3	—	$2\pi^2 390\,625/26\,068 \approx 295.8$
2.5	2	—	$2\pi^2 200\,000/21\,609 \approx 182.7$
3	5/3	—	$2\pi^2 253\,125/17\,024 \approx 293.5$
3	2	—	$2\pi^2 324/35 \approx 182.7$
4	5/3	—	$2\pi^2 5120/323 \approx 312.9$
4	2	—	$2\pi^2 131\,072/13\,125 \approx 197.1$

TABLE 3. Reference values for I_{SM} and I_H for different combinations of α and s .

range; see figure 1(a).

The former ratio, I_H/I_H^{ref} , varies only little, because the Hosking integral is always reasonably well conserved, except when the magnetic diffusivity is large. Near $\eta k_0^2 \approx 0.1$, the ratio has for all runs a well-distinguished maximum, which is the value we quote in table 2. These values tend to be approximately 20 % larger than those at the end of the run, which are the reference values given in table 2.

It is interesting to note that I_H/I_H^{ref} is approximately twice as large on the finer mesh (run C) than on the coarser mesh (run D). This is somewhat surprising. It should be noted, however, that run C with a larger mesh had actually a larger magnetic diffusivity ($\eta k_0/c_s = 7 \times 10^{-3}$) than run D ($\eta k_0/c_s = 5 \times 10^{-5}$); see table 2. It is therefore possible that run D was actually underresolved and that this was not yet noticed.

3.4. Comments on non-Gaussianity

The question of non-Gaussianity is important in many aspects of cosmology. Not all of its aspects are captured by kurtosis or skewness. In the work of Zhou *et al.* (2022), it was already pointed out that, although the kurtosis was only slightly below the Gaussian value of three, there was a very strong effect on the statistics of the fourth-order moments that enter in the calculation of I_H and $Sp(h)$. In figure 3, we compare $Sp(h)$ at the initial and a later time from the numerical calculation and the semi-analytical calculation based on the actual magnetic energy spectra, assuming Gaussian statistics. As in Zhou *et al.* (2022), we find also here a tenfold excess of the actual spectra compared with the value expected based on the assumption of Gaussianity.

3.5. Scaling for non-integer values of α

We now address in more detail the case $\alpha = 1.7$, for which (2.9) with $\beta = 3/2$ would predict $\lim_{k \rightarrow 0} E_M(k, t) \propto t^{4\alpha/9 - 2/3} = t^{4/45} \approx t^{0.09}$. These runs are listed in table 2 as runs O and P. We have seen that, for small magnetic diffusivity, I_H is well conserved for all values of α . On the other hand, I_{SM} appears to be well conserved in the special case of $\alpha = 2$. One possibility is therefore that, as long as $\alpha > 2$, we have an inverse cascade, but not for $\alpha \leq 2$. However, the argument for not expecting an inverse cascade relies heavily on the existence of I_{SM} and that it is non-vanishing. If we accept that, for $\alpha = 3$, $Sp(\mathbf{B})$ cannot be expanded in terms of k^2 and k^4 , then this would also be true for $\alpha = 1.7$, which is a value between $3/2$ and 2 . One might therefore expect that, also in this case, I_{SM} would not be

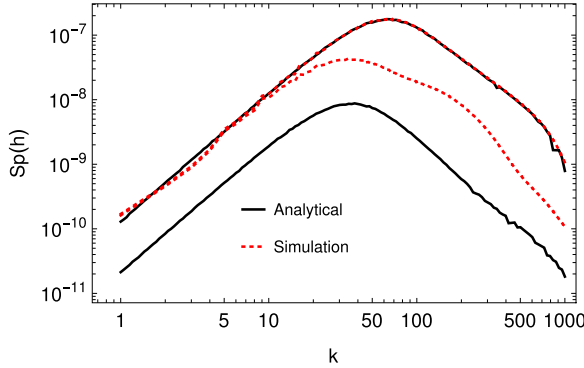


FIGURE 3. The function $Sp(h)$ at $t = 0$ and 1. The dotted red curves represent the spectra obtained from the simulation and the solid black curves represent the spectra calculated by assuming the magnetic field distribution to be Gaussian.

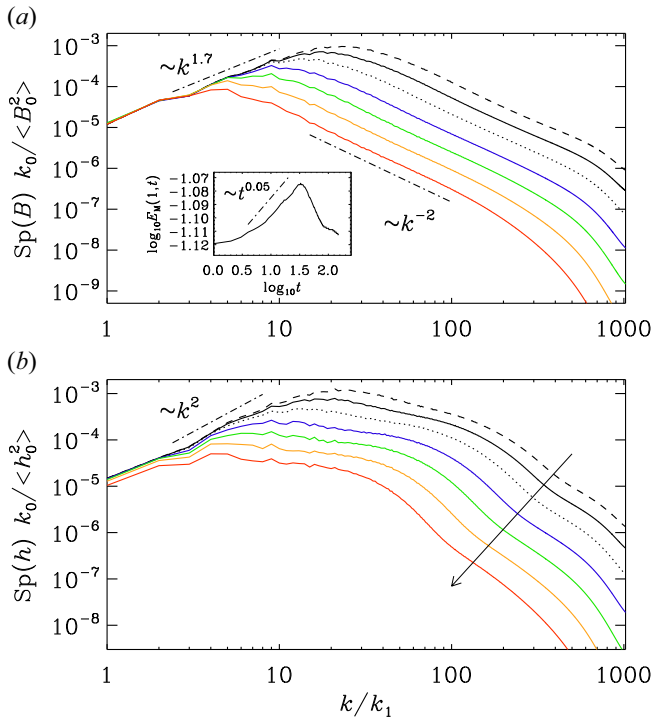


FIGURE 4. Similar to figure 1, but for $\alpha = 1.7$.

conserved, and that the decay is governed by the conservation of I_H . This possibility was already listed table 1.

In figure 4(a) we show that there is no noticeable growth of $\lim_{k \rightarrow 0} E_M(k, t)$. The inset, however, does show that there is an intermediate phase with a very weak growth $\propto t^{0.05}$. Given that the theoretically expected growth $\propto t^{0.09}$ is already very small, and that the degree of conservation of I_H is also limited by a finite Reynolds number, as seen in figure 4(b) showing a premature decline of $Sp(h)/k^2$ in time at small k , it is indeed possible

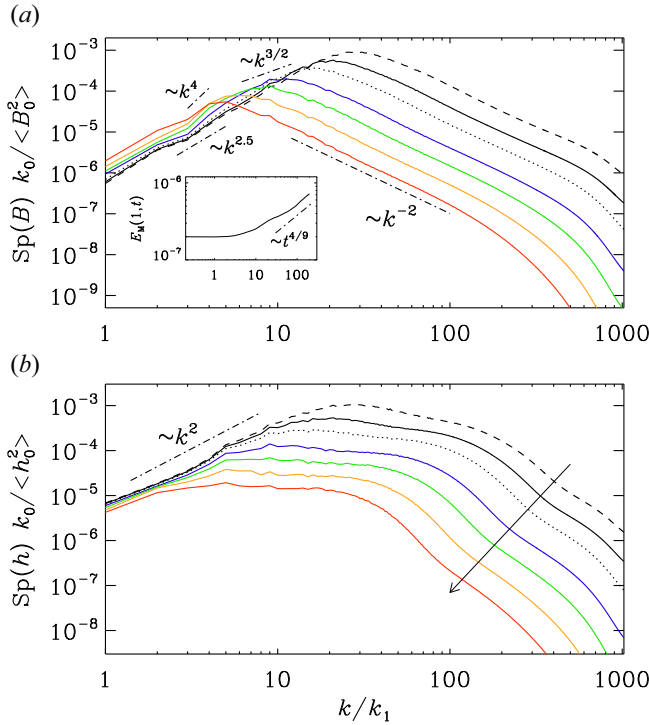


FIGURE 5. Similar to figure 1, but for $\alpha = 2.5$. Note that, for the green line at $t = 50$, there is some evidence for a short range with a steeper spectrum, possibly $\propto k^4$.

that, at larger resolution and smaller magnetic diffusivity, clearer inverse cascading might emerge.

Next, we consider the case $\alpha = 2.5$. The results are shown in figure 5. We see inverse cascading that is compatible with $a_{2.5}(t) \propto t^{4/9} = t^{0.44}$. Note that, for the intermediate time $t = 50$, there is some evidence for a short range with a steeper spectrum, but it would hardly be as steep as k^4 .

3.6. Reassessment of the Saffman case

Given that there is now some evidence for inverse cascading for $\alpha = 1.7$, it is reasonable to re-address earlier evidence for the absence of inverse cascading for $\alpha = 2$. We must remember that the results of Brandenburg & Larsson (2023) for $\alpha = 2$ were obtained at a resolution of 1024^3 mesh points using a value of the magnetic Reynolds number that was possibly too large for that resolution. More importantly, however, a superficial inspection of the spectral evolution may not suffice. We have therefore repeated such a calculation using otherwise the same parameters as in figures 1, 4 and 5 and compared the evolution of the spectral magnetic energy at low k with that expected theoretically. Our initial result suggested that a larger scale separation would be needed to obtain reliable results; see Appendix B.

A large scale-separation ratio, k_0/k_1 , was previously found to be important. For example, in the context of the Hall cascade, a threefold larger value of k_0/k_1 was needed to demonstrate clear evidence for inverse cascading (Brandenburg 2020). Therefore, we now present in figure 6 the results for $k_0 = 180 k_1$. We see that, similarly to the case of $\alpha = 1.7$ in the inset of figure 4(a), there is an initial rise of spectral magnetic energy compatible

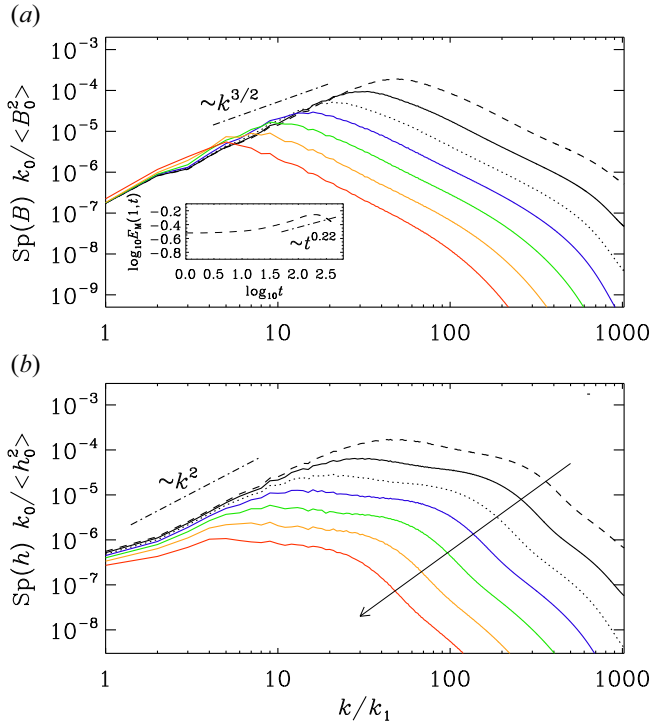


FIGURE 6. Similar to figure 1, but for $\alpha = 2$ and $k_0 = 180 k_1$ at $t = 2, 6, 15, 34, 80, 183$ and 416 . The inset applies here to the evolution at $k = 5 k_1$, instead of $k = k_1$, as for all other plots.

with being $\propto t^{0.22}$, which, again, is followed by a decline at very late times. This result therefore supports the notion that the Hosking integral is indeed well conserved and that it governs the evolution of the magnetic field even for $\alpha = 2$.

3.7. Evolution in the pq diagram

There is a range of tools for assessing the decay properties of MHD turbulence. We have already discussed the determination of I_H and I_{SM} , and the potentially universal coefficients $C_H^{(\xi)}$, $C_H^{(E)}$ and $C_H^{(E)}$. We also discussed the close relation between the envelope parameter β in (2.7) and (3.1a–c), and the parameter q characterizing the growth of the correlation length $\xi_M \propto t^q$. There is also the parameter p characterizing the decay of magnetic energy, $\mathcal{E}_M \propto t^{-p}$. Both p and q can also be determined as instantaneous scaling parameters through $p(t) = -d \ln \mathcal{E}_M / d \ln t$ and $q(t) = d \ln \xi_M / d \ln t$, and their parametric representation $p(t)$ vs $q(t)$ gives insights into the properties of the system and how far it is from a self-similar evolution (Brandenburg & Kahniashvili 2017) and the scale-invariance line, $p = 2(1 - q)$; see Zhou *et al.* (2022).

In figure 7, we show such a pq diagram for runs B, C and Q. We see that the points (q, p) for different times and for both runs cluster around $(q, p) = (4/9, 10/9)$, as expected for Hosking scaling. The locations for Loitsyansky and Saffman scalings, $(2/7, 10/7)$ and $(2/5, 6/5)$, respectively, as well as for the fully helical case $(2/3, 2/3)$, are also indicated for comparison. Note that, even for run Q with $\alpha = 2$, the points are closer to Hosking scaling than to Saffman scaling.

A detailed assessment of the full range of scaling parameters is important for establishing the validity of Hosking scaling. Assessments based on comparisons of the

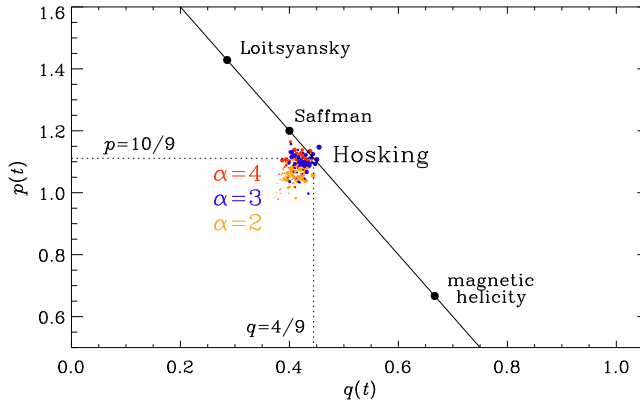


FIGURE 7. A pq diagram showing a parametric representation of $p(t)$ vs $q(t)$ for runs B ($\alpha = 3$, blue), C ($\alpha = 4$, red) and Q ($\alpha = 2$, orange) and $10 < t < 60$. Larger symbols correspond to later times. The locations for Loitsyansky and Saffman scalings, as well as for the fully helical case, are indicated as black dots along the scale-invariance line (black solid line), $p = 2(1 - q)$, and the black dotted lines mark the position $q = 4/9$ and $p = 10/9$.

parameter p for different runs may not be sufficient, and have not yet confirmed this scaling; see Armua, Berera & Calderón-Figueroa (2023) for recent results. Thus, the idea behind the Hosking phenomenology is therefore not universally accepted. Possible reasons for discrepancies could lie in an insufficiently large magnetic Reynolds number and therefore also in a lack of a sufficiently long inertial range. Therefore, it would be useful to have independent verification from other groups. In this connection, it should be noted that additional support for the validity of the Hosking scaling came from two rather different numerical experiments. First, in applications to the Hall cascade, the Hosking phenomenology predicts the scalings $q = 4/13$ and $p = 10/13$, which was confirmed by simulations (Brandenburg 2023). Second, in relativistic plasmas where the mean magnetic helicity density is finite, but the total chirality vanishes because the helicity is exactly balanced by fermions chirality, the Hosking phenomenology predicts a decay of mean magnetic helicity $\propto t^{-2/3}$, which, again, was confirmed by simulations (Brandenburg, Kamada & Schober 2023).

4. Conclusions

Our work has shown that the decay dynamics of an initial magnetic field with power-law scaling proportional to k^3 is similar to that for k^4 . According to a simple argument involving self-similarity, we showed and confirmed that the temporal growth of the magnetic energy spectra at small k is proportional to $t^{4\alpha/9-2/3}$, so for $\alpha = 3$, we have an increase proportional to $t^{2/3}$, while for $\alpha = 4$, the increase is proportional to $t^{10/9}$. Thus, although we cannot exclude the possibility of artefacts from the finite size of the computational domain, our simulations now suggest inverse cascading even for an initial Saffman spectrum. This underlines the importance of the Hosking integral in determining the decay dynamics for a large class of initial magnetic energy spectra. We also confirmed that the non-dimensional coefficients in the empirical scaling relations for $\xi_M(t)$, $\mathcal{E}_M(t)$ and $E_M(k, t)$ are compatible with those found earlier for an initial k^4 subinertial range spectrum.

At the moment, even with a resolution of 2048^3 mesh points, we cannot make very firm statements about the case $\alpha = 1.7$, because I_H is not sufficiently well conserved and the

value of α is close to $3/2$. It would be useful to reconsider the case $\alpha = 2$ with even higher resolution to confirm the violation of the conservation of the magnetic Saffman integral, and thus weak inverse cascading $\propto t^{0.2}$.

Acknowledgements

We are grateful to D. Hosking, A. Midiri, A. Roper Pol and K. Subramanian for encouraging discussions. We are also grateful to H. Zhou for his suggestion to consider steeper spectra, as we have now discussed in [Appendix A](#). We thank the two referees for useful suggestions and comments that have led to improvements of the paper. R.S. acknowledges the funding support provided by the ERC HERO-810451 grant. T.V. thanks CERN for hospitality during the course of this work.

Editor A. Schekochihin thanks the referees for their advice in evaluating this article.

Funding

A.B. and R.S. were supported in part by the Swedish Research Council (Vetenskapsrådet, 2019-04234); Nordita is sponsored by Nordforsk. T.V. was supported by the U.S. Department of Energy, Office of High Energy Physics, under Award No. DE-SC0019470. We acknowledge the allocation of computing resources provided by the Swedish National Allocations Committee at the Centre for Parallel Computers at the Royal Institute of Technology in Stockholm and Linköping.

Declaration of interests

The authors report no conflict of interest.

Data availability statement

The data that support the findings of this study are openly available on Zenodo at [doi:10.5281/zenodo.8128611](https://doi.org/10.5281/zenodo.8128611) (v2023.07.09). All calculations have been performed with the PENCIL CODE (Pencil Code Collaboration *et al.* 2021); [DOI:10.5281/zenodo.3961647](https://doi.org/10.5281/zenodo.3961647).

Appendix A. Approach to a k^4 spectrum from a steeper one

In this paper, we focus on the case $\alpha < 4$. This is because for $\alpha = 4$, the spectrum quickly develops into one that is equivalent to $\alpha = 4$. The approach to a k^4 spectrum from a steeper k^6 spectrum is shown in [figure 8](#). We see that the spectra quickly gain power at low k so that the subinertial range is $\propto k^4$. This happens at very early times, well before any inverse cascading has started yet.

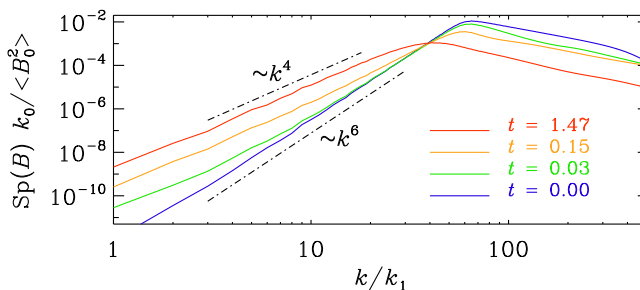


FIGURE 8. Approach to a k^4 spectrum from a steeper k^6 spectrum for $k_0 = 60k_1$ using 1024^3 mesh points and otherwise the same parameters as for [figure 1](#).

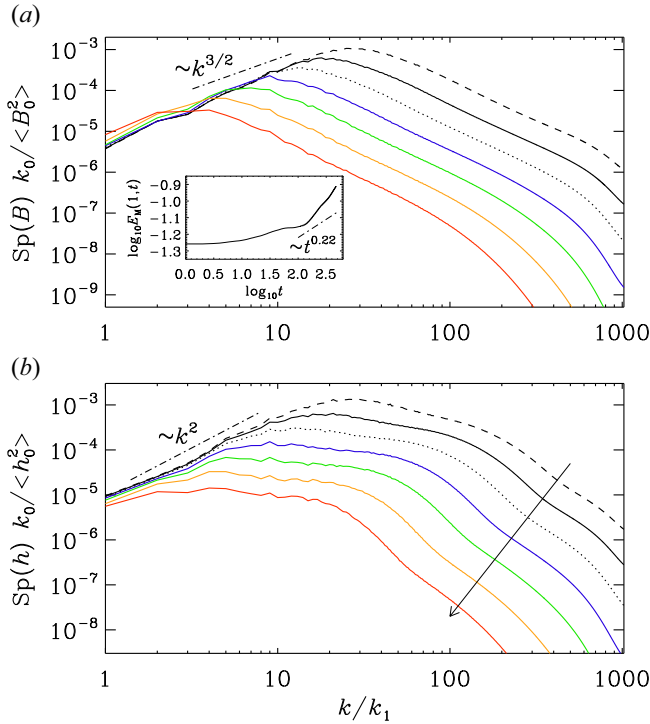


FIGURE 9. Similar to figure 1, but for $\alpha = 2$ and at $t = 2, 6, 15, 37, 87, 205$ and 475 and with $k_0 = 60 k_1$.

Appendix B. Finite-size effects

In § 3.6, we mentioned that we needed a larger scale-separation ratio to obtain reliable results for $\alpha = 2$. To demonstrate the problem, we show here the result for the usual scale separation of $k_0/k_1 = 60$. The inset to figure 9(a) shows that the growth of $E_M(k, t)$ at $k = k_1$ does not follow a clear power-law scaling. There is a decline in the slope in the range $50 < t < 100$, followed by an increase that lasts until the end of the simulation at $t = 475$. A likely explanation for this unexpected behaviour could be finite-size effects. If that is the case, the intermediate decline in the slope could be interpreted as evidence for a levelling off, compatible with Saffman scaling.

We should also mention that it turned out that, even for $k_0 = 60 k_1$, we had to decrease the initial magnetic field strength to $v_{A0}/c_s \approx 0.65$ to prevent the code from crashing. This value of v_{A0}/c_s is approximately 30 % smaller than our usual value of $v_{A0}/c_s \approx 0.87$ that was used for the other runs at that resolution. While these field strengths are not that different, it indicates that at early times, our simulations are close to the limit below which we can still trust them.

REFERENCES

ARMUA, A., BERERA, A. & CALDERÓN-FIGUEROA, J. 2023 Parameter study of decaying magnetohydrodynamic turbulence. *Phys. Rev. E* **107** (5), 055206.
 BATCHELOR, G.K. 1953 *The Theory of Homogeneous Turbulence*. Cambridge University Press.
 BERGER, M.A. 1984 Rigorous new limits on magnetic helicity dissipation in the solar corona. *Geophys. Astrophys. Fluid Dyn.* **30** (1), 79–104.

- BHAT, P., ZHOU, M. & LOUREIRO, N.F. 2021 Inverse energy transfer in decaying, three-dimensional, non-helical magnetic turbulence due to magnetic reconnection. *Mon. Not. R. Astron. Soc.* **501** (2), 3074–3087.
- BRANDENBURG, A. 2001 The inverse cascade and nonlinear alpha-effect in simulations of isotropic helical hydromagnetic turbulence. *Astrophys. J.* **550** (2), 824–840.
- BRANDENBURG, A. 2020 Hall cascade with fractional magnetic helicity in neutron star crusts. *Astrophys. J.* **901** (1), 18.
- BRANDENBURG, A. 2023 Hosking integral in non-helical Hall cascade. *J. Plasma Phys.* **89** (1), 175890101.
- BRANDENBURG, A. & KAHNIASHVILI, T. 2017 Classes of hydrodynamic and magnetohydrodynamic turbulent decay. *Phys. Rev. Lett.* **118**, 055102.
- BRANDENBURG, A., KAHNIASHVILI, T., MANDAL, S., ROPER POL, A., TEVZADZE, A.G. & VACHASPATI, T. 2017 Evolution of hydromagnetic turbulence from the electroweak phase transition. *Phys. Rev. D* **96** (12), 123528.
- BRANDENBURG, A., KAMADA, K. & SCHOBER, J. 2023 Decay law of magnetic turbulence with helicity balanced by chiral fermions. *Phys. Rev. Res.* **5** (2), L022028.
- BRANDENBURG, A. & LARSSON, G. 2023 Turbulence with magnetic helicity that is absent on average. *Atmosphere* **14** (6), 932.
- DURRER, R. & CAPRINI, C. 2003 Primordial magnetic fields and causality. *J. Cosmol. Astropart. Phys.* **2003** (11), 010.
- FRISCH, U., POUQUET, A., LEORAT, J. & MAZURE, A. 1975 Possibility of an inverse cascade of magnetic helicity in magnetohydrodynamic turbulence. *J. Fluid Mech.* **68**, 769–778.
- HOSKING, D.N. & SCHEKOCHIHIN, A.A. 2021 Reconnection-controlled decay of magnetohydrodynamic turbulence and the role of invariants. *Phys. Rev. X* **11** (4), 041005.
- HOSKING, D.N. & SCHEKOCHIHIN, A.A. 2023 Cosmic-void observations reconciled with primordial magnetogenesis. [arXiv:2203.03573](https://arxiv.org/abs/2203.03573).
- KOLMOGOROV, A. 1941 The local structure of turbulence in incompressible viscous fluid for very large Reynolds' numbers. *Dokl. Akad. Nauk SSSR* **30**, 301–305.
- MATTHAEUS, W.H. & GOLDSTEIN, M.L. 1982 Measurement of the rugged invariants of magnetohydrodynamic turbulence in the solar wind. *J. Geophys. Res.* **87** (A8), 6011–6028.
- MOFFATT, H.K. 1969 The degree of knottedness of tangled vortex lines. *J. Fluid Mech.* **35**, 117–129.
- PARKER, E.N. 1979 *Cosmical Magnetic Fields. Their Origin and Their Activity*. Clarendon Press.
- PATEL, T. & VACHASPATI, T. 2022 Kibble mechanism for electroweak magnetic monopoles and magnetic fields. *J. High Energy Phys.* **01**, 059.
- PENCIL CODE COLLABORATION, BRANDENBURG, A., JOHANSEN, A., BOURDIN, P., DOBLER, W., LYRA, W., RHEINHARDT, M., BINGERT, S., HAUGEN, N., MEE, A., *et al.* 2021 The Pencil Code, a modular MPI code for partial differential equations and particles: multipurpose and multiuser-maintained. *JOSS* **6** (58), 2807.
- POUQUET, A., FRISCH, U. & LEORAT, J. 1976 Strong MHD helical turbulence and the nonlinear dynamo effect. *J. Fluid Mech.* **77**, 321–354.
- REPPIN, J. & BANERJEE, R. 2017 Nonhelical turbulence and the inverse transfer of energy: a parameter study. *Phys. Rev. E* **96** (5), 053105.
- SAFFMAN, P.G. 1967 The large-scale structure of homogeneous turbulence. *J. Fluid Mech.* **27**, 581–593.
- SCHEKOCHIHIN, A.A. 2022 MHD turbulence: a biased review. *J. Plasma Phys.* **88** (5), 155880501.
- STEENBECK, M., KRAUSE, F. & RÄDLER, K.H. 1966 Berechnung der mittleren Lorentz-Feldstärke für ein elektrisch leitendes Medium in turbulenter, durch Coriolis-Kräfte beeinflusster Bewegung. *Z. Naturforsch. A* **21**, 369.
- SUBRAMANIAN, K. 2019 From primordial seed magnetic fields to the galactic dynamo. *Galaxies* **7** (2), 47.
- VACHASPATI, T. 2021 Progress on cosmological magnetic fields. *Rep. Prog. Phys.* **84** (7), 074901.
- WOLTJER, L. 1958 A theorem on force-free magnetic fields. *Proc. Natl Acad. Sci.* **44** (6), 489–491.
- ZHOU, M., BHAT, P., LOUREIRO, N.F. & UZDENSKY, D.A. 2019 Magnetic island merger as a mechanism for inverse magnetic energy transfer. *Phys. Rev. Res.* **1** (1), 012004.
- ZHOU, M., LOUREIRO, N.F. & UZDENSKY, D.A. 2020 Multi-scale dynamics of magnetic flux tubes and inverse magnetic energy transfer. *J. Plasma Phys.* **86** (4), 535860401.
- ZHOU, H., SHARMA, R. & BRANDENBURG, A. 2022 Scaling of the Hosking integral in decaying magnetically dominated turbulence. *J. Plasma Phys.* **88** (6), 905880602.